MIT Libraries | DSpace@MIT

MIT Open Access Articles

High-Resolution Physically-Windowed Sensors for Power Electronics Applications

The MIT Faculty has made this article openly available. ***Please share*** how this access benefits you. Your story matters.

Citation: Wichakool, Warit et al. "High-resolution Physically-windowed Sensors for Power Electronics Applications." 2010 Twenty-Fifth Annual IEEE Applied Power Electronics Conference and Exposition, IEEE, 2010. 580–587. © Copyright 2010 IEEE

As Published: http://dx.doi.org/10.1109/APEC.2010.5433611

Publisher: Institute of Electrical and Electronics Engineers (IEEE)

Persistent URL: http://hdl.handle.net/1721.1/72127

Version: Final published version: final published article, as it appeared in a journal, conference proceedings, or other formally published context

Terms of Use: Article is made available in accordance with the publisher's policy and may be subject to US copyright law. Please refer to the publisher's site for terms of use.

Massachusetts Institute of Technology

High-resolution Physically-windowed Sensors for Power Electronics Applications

Warit Wichakool, James Paris, Al-Thaddeus Avestruz, Dr. Steven B. Leeb

***Abstract*—This paper presents a high-resolution, physically-windowed sensor architecture that is well-suited for energy scorekeeping and diagnostic applications. The sensor can track a large-scale main signal while capturing small-scale variations. The prototype system measures a small current signal using a closed-loop Hall sensor, and extends the range by driving a compensation current through an auxiliary winding. The system combines the compensation command and the sampled output of the residual sensor to reconstruct the input signal. Results show that the prototype can measure both dc and ac currents with 10 mA resolution over a 160 A current range.**

I. Introduction

In energy scorekeeping and diagnostic applications, current sensors are often deployed to collect and analyze current waveforms from a collection of loads [1]. Analysis provides load disaggregation and detection, power consumption profiling, and diagnostics based on electrical signatures [1]–[5]. Many current sensors are available according to dynamic range and sensitivity. Hall sensors, fluxgate-based sensors, and Rogowski coils have all been used for non-contact current measurement [6]–[12]. As monitoring systems grow to include more loads and to provide more detailed information about the loads, the scalability and utility of the system depends on the quality of data acquired by the current sensor [13]. When monitoring large loads or collections of loads, some relevant features may be found in harmonic or aperiodic content that is small compared to the current drawn at the fundamental line frequency. For other features, the full amplitude signal may be required.

A physically-windowed sensor architecture is introduced that allows for a more flexible tradeoff between sensitivity and dynamic range. Large-scale variations are cancelled such that the measured signal remains within a small operating window, while the residual small-scale signals are sensed conventionally with an accurate sensor. This architecture is similar to that of pipelined analog-to-digital converters [14], but utilizes a physical cancellation approach that can be applied to magnetic flux-based current sensors, strain gauges, pressure transducers, and many other physical systems. The cancellation is software-controlled by an embedded microcontroller, permitting a variety of windowing techniques and flexible processing and analysis.

In this paper, we present an initial application of this concept to power electronics by developing a physically-windowed current sensor that demonstrates high accuracy over a wide input range.

II. System Design

Our architecture uses an additional physical input to apply a cancellation signal to a sensor. This enables an accurate but narrow-range sensor to measure effectively beyond its specified operating range. The initial implementation applies this approach to a current sensor and follows the overall design shown in Fig. 1. A compensation current i_{comp} is driven anti-parallel to large input currents such that the effective total current i_{meas} seen by the sensing element remains within its designated operating range. The microcontroller coordinates and controls the system, performing calibration at startup and adjusting the compensation as necessary to keep the sensor at the desired operating point.

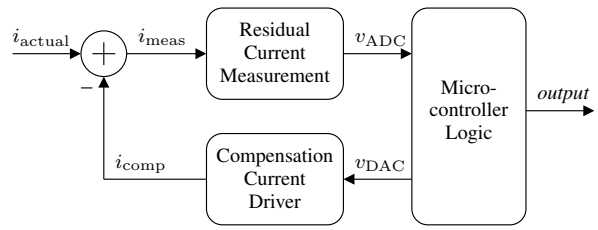

Fig. 1. System block diagram. The system consists of three primary components: the compensation current driver, the residual current measurement, and the microcontroller logic. The compensation current i_{comp} is subtracted from the primary input current i_{actual} by physical cancellation of magnetic flux.

A. Signal Reconstruction

Fig. 2 depicts the signal reconstruction used to determine the total current using the windowed measurement. The total input current i_{actual} is calculated from the instantaneous compensation current and sensor measurement as

$$i_{\mathrm{actual}} = k_c \cdot i_{\mathrm{comp}} + k_m \cdot i_{\mathrm{meas}}, \tag{1}$$

where k_c and k_m are calibration values determined by physical factors such as the number of turns on the sensing core and the amount of magnetic coupling between coils.

The compensation current i_{comp} is generated by an operational transconductance amplifier (OTA), detailed in §IV-B. This current i_{comp} is set by the microcontroller using a digital-to-analog converter (DAC) command voltage, v_{DAC}. The total compensation current is given by

$$i_{\mathrm{comp}} = k_{\mathrm{DAC}} \cdot v_{\mathrm{DAC}}, \tag{2}$$

where k_{DAC} is determined by the OTA design.

Residual current is measured using a closed-loop Hall sensor, detailed in §IV-A. This current i_{meas} is read from an analog-to-digital converter (ADC) as the voltage v_{ADC}, and is given by

$$i_{\mathrm{meas}} = k_{\mathrm{ADC}} \cdot v_{\mathrm{ADC}}, \tag{3}$$

where k_{ADC} is determined by the sensor front-end design.

978-1-4244-4783-1/10/$25.00 ©2010 IEEE

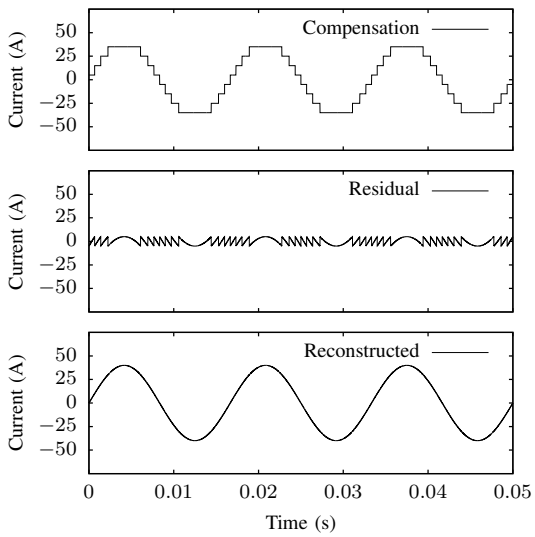

Fig. 2. Signal reconstruction. The compensation current and measured residual current are combined to determine the total current through the full sensor.

Combining these equations, the complete reconstruction is

$$i_{\text{actual}} = k_c \cdot k_{\text{DAC}} \cdot v_{\text{DAC}} + k_m \cdot k_{\text{ADC}} \cdot v_{\text{ADC}}.$$

The constants can be simplified as:

$$i_{\text{actual}} = k_s(v_{\text{DAC}} + k_r \cdot v_{\text{ADC}}), \tag{4}$$

where k_r represents the ratio between the DAC command voltage and the corresponding change in ADC input voltage, and k_s represents a scaling to convert to actual current. This simplified form is used both for discussion and by the internal calibration and windowing procedures described in §IV-C.

B. Resolution and Range

The performance of the overall physically-windowed sensor system is determined by the parameters of its components. The ranges and resolutions of the compensation current and the residual measurement overlap, as depicted in Fig. 3. In this example, the ADC is accurate to 11 bits over a range of 5 A, while the DAC command is accurate to 10 bits over a range of 160 A. The amount of overlap directly relates to the parameters k_r and k_s in (4).

A key requirement for physically windowed sensing is that the compensation output must remain stable and predictable to the full system resolution. In Fig. 3, this requirement is depicted as a dashed line on the DAC output. Here, for the lowest-order bits of the combined result to be accurate, each of the 2^{10} possible DAC commands must result in a voltage stability of one part in 2^{16}. Certainly, a 16-bit DAC would suffice. However, only stability is needed, not accuracy. If a lower-resolution DAC is, or can be made to be, similarly stable in output, it is sufficient for the sensor architecture. Using such

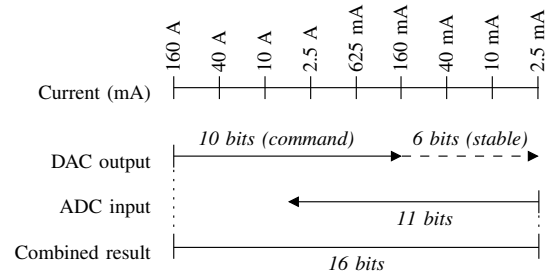

Fig. 3. Overlap of the DAC output, relating to compensation current, and the ADC input, relating to the residual measurement. The ranges and overlapped positions are related to the parameters in (4). The combined result shows high accuracy over the full range.

a DAC may provide cost or performance benefits.[1]

Given that the stability requirement is met, then the actual output voltage v_{DAC} can be related to the DAC command x as

$$v_{\text{DAC}}(x) \propto \frac{x}{2^{10}} + \frac{\text{LOOKUP}[x]}{2^{16}} \tag{5}$$

where $\text{LOOKUP}[x]$ is a 2^{10}-entry table that stores these 6 extra stable bits. This table can be populated by the microcontroller in a calibration step that uses the ADC input to determine the low-order bits of each DAC output.

C. Windowing

The front-end current measurement is "windowed" by the compensation current in the sense that the compensation sets a particular operating point, and the Hall sensor measures a small window of current around this point. The microcontroller has significant flexibility in the windowing approach, and the behavior can be adjusted based on expected workloads and system parameters.

A basic approach to windowing is to continuously recenter the window so that the ADC measurement is zeroed; that is, the residual current is driven to zero after each sample. However, this requires that the OTA change its current output nearly continuously as the input signal changes, increasing the bandwidth requirements and potentially making the data less accurate if changes in compensation current are slow to settle.

The approach demonstrated by the reconstruction in Fig. 2 is to change the DAC command when the residual current in the sensor approaches the limits of the front-end. The compensation current will remain constant for small input signal changes, and only change for larger input signals that exceed the window. For many input signals, this may allow the compensation to change relatively slowly, reducing bandwidth requirements for the compensation driver.

More advanced approaches are possible, particularly for loads with known characteristics. A predictive estimator in the microcontroller can perform an anticipatory change in the compensation current so that the residual sensor current would

[1]The prototype implementation in §IV simulates this stability by using a 16-bit DAC with fixed random low-order bits on a 10-bit command. The low-order bits are set by the microcontroller and can be adjusted for testing purposes.

be expected to fall within the sensor limits at the next sample interval. Such techniques can potentially increase the slew rate capability of the system.

D. Bandwidth

The bandwidth of the physically windowed sensor system depends on the input signals and their relation to the sensor window. There are two fundamental regions of operation: the first, within the windowed range of the residual current measurement, and the second, over the full range of the compensation current. For input currents that fall entirely within the window, the bandwidth performance of the system is equal to that of the residual current sensor front-end, as the compensation current is held constant. For full-scale input signals, the bandwidth is instead limited by how fast the compensation current can track the input change.

Maximum slew rate may be further affected by the windowing algorithm in use. Once the residual current exceeds the range of the sensor window, the compensation command must be adjusted. In the absence of prediction, the microcontroller will not know by how much the residual current exceeded the window, and will be limited to stepping the compensation by one "window" worth of current at a time. This, combined with the sampling rate of the residual sensor and the bandwidth of the compensation driver, will set the maximum $\frac{di}{dt}$ that can be accurately tracked. For slew rates outside this limit, the subsequent front-end sample will still exceed the window, and the microcontroller can report the potential inaccuracy as part of the output data stream.

The bandwidth and slew rate limits are a function of the resolution, range, and bandwidth of the system components. Flexible tradeoffs can be made by, for example, adjusting the system to increase k_r in (4). This would have the effect of increasing the relative size of the sensor window, increasing the region in which the recorded signal retains full bandwidth, and increasing the maximum slew rate. Conversely, increasing k_r increases the overall resolution of the reconstructed signal.

III. Benefits and Motivation

In many physical systems, large-scale changes occur at relatively slow speed while small-scale details can change rapidly. For example, an electric motor draws a 60 Hz fundamental current from the utility, but it may be desirable to observe a principal slot harmonic (PSH) at several hundreds or thousands of Hertz to track the motor speed [15]. These small, high-frequency details are superimposed on top of the 60 Hz current and need to be examined without saturating the sensor front-end. Conventional current sensors like the closed-loop Hall-effect sensor utilize a single compensation circuit to measure current. The physically-windowed sensing system, instead, divides the measurement into two subsystems, the compensation current driver and the residual current measurement. By dividing the problem and taking advantage of the fundamental differences between the requirements of the large-scale and small-scale measurements, the windowed system can utilize power and bandwidth trade-offs in the design of design each subsystem. This section describes these trade-offs and their design considerations.

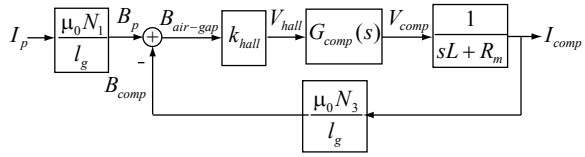

Fig. 4. Typical design for a closed-loop hall sensor, with one compensation circuit.

A. Resolution

To obtain an accurate measurement, the system needs a reference that is stable to the required resolution specification. A conventional current sensor can utilize a single high-resolution ADC to perform the measurement, or it can use a single high-resolution DAC as a reference against which to compare a measurement. In both cases, it is required that the ADC or DAC be both stable and accurate to the full resolution.

With the physically-windowed approach, it is sufficient that the DAC be stable, but not necessarily accurate. A DAC with fewer controllable bits, but stable to the full resolution, can still be used. Initial experiments, testing the output voltage of a 16-bit AD7846 DAC with a HP34401A multimeter, demonstrated an accuracy of approximately 26 μV on a ±5 V range, or approximately 18.5 bits, in a controlled environment. This example shows that, under some conditions, the output of the DAC is more stable than the controllable input.

The physically-windowed sensor design can then use a moderately accurate DAC and a moderately accurate ADC to create a compound data acquisition system that can accurately resolve more than the number of bits provided by either the DAC or ADC alone. For example, assuming proper calibration is performed, the system may be able to use one 10-bit DAC and one 10-bit ADC to create an effective 12-bit data acquisition system.

B. Bandwidth

A key element in the design process for analog circuits is the trade-off between power consumption and bandwidth. If the signal of interest is comprised of both low-frequency and high-frequency content, the current sensor may be able to take advantage of this separation by utilizing two separate compensation circuits, each optimized for one frequency region.

The basic topology of a typical current sensor based on zero-flux sensing consists of three parts: a magnetic flux sensor, a compensation circuit, and a compensation winding. The system block diagram is shown in Fig. 4. The input current creates a magnetic flux which is focused in the air gap of the gapped magnetic core. The magnetic flux sensor senses any magnetic flux in the air gap, and provides an output signal for the compensation circuit. This circuit drives a cancellation current to cancel the magnetic flux. Effectively, the system forces the magnetic flux in the air gap to zero, keeping the magnetic core around the zero-flux operating point and away from the saturation region.

In order to measure a fast dynamic signal accurately, the measuring system is required to have a wide bandwidth and

a large open-loop gain. In another words, the gain-bandwidth product of the open-loop transfer function must be very large. As shown in Fig. 4, the system can be designed to meet the large gain-bandwidth product by choosing an appropriate compensation circuit $G_{\mathrm{comp}}(s)$. A typical compensator is an integrator with a lead compensation. The integrator provides a large open-loop gain at low frequency, whereas the lead compensation provides stability for the system. A typical transfer function of the lead-compensated integrator circuit can be described as

$$G_{comp}(s) = \frac{(s\tau_2 + 1)}{(s\tau_1 + 1)}, \tag{6}$$

where $\frac{1}{\tau_1}$ is a low frequency pole of a practical integrator circuit, and $\frac{1}{\tau_2}$ is the compensated zero. In this case, we assume that all high frequency poles of the op-amp and parasitics are negligible at the cross-over frequency. The compensation circuit would be designed to meet the required bandwidth of the input signal.

The compensation circuit must cancel the flux by driving an equivalent current through the magnetic core, typically using an output stage consisting of an operational amplifier and push-pull buffer circuit. If the compensation current coil consists of N_3 turns, the primary winding consists of N_1 turns, and the maximum input current is $i_{\mathrm{actual_max}}$, then the compensation circuit must be able to drive $\frac{N_1}{N_3} i_{\mathrm{actual_max}}$ through the coil.

As N_3 is increased, the drive current is lowered, but this also affects the inductance that the compensation circuit has to drive. Specifically, the inductance of the compensation coil is proportional to ${N_3}^2$. Large inductance will limit the maximum slew rate that the buffer circuit can provide for compensation. The slew rate $\frac{di}{dt}$ of the current in an inductor is given by

$$\frac{di}{dt} = \frac{v_L}{L} \propto \frac{v_{supply}}{{N_3}^2}, \tag{7}$$

where v_L represents the voltage across the inductor, which is limited by the supply voltage of the system. Given the same supply voltage, a smaller inductance will allow the system to follow the input current more accurately.

The physically-window sensing system, on the other hand, divides the compensation circuit into two parts: a large, slow compensation circuit for the bulk of the flux cancellation, and a small, fast compensation circuit for measuring the residual. Block diagrams of the proposed system are shown in Fig. 5.

For the smaller residual measuring range, the compensation circuit can have the same design as the single compensation circuit case. Since the maximum current output is reduced, the number of winding turns N_3 can be reduced, effectively lowering the inductance of the coil. The lower inductance allows this compensation circuit to follow the higher $\frac{di}{dt}$ rate according to (7), given the same supply voltage.

The auxiliary compensation circuit must provide a cancellation current for a larger portion of the magnetic flux in the core. Specifically, the auxiliary compensation circuit is responsible for providing a cancellation current of $\frac{N_1}{N_2} i_{\mathrm{actual_max}}$ where N_2 is the number of turns in the auxiliary winding. This is analogous to the requirement of the first compensation

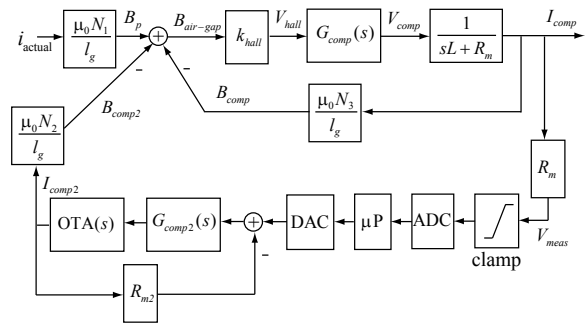

Fig. 5. Physically windowed current sensor, with two compensation circuits.

circuit, and the circuit can be made similarly, with minor adjustments. In our prototype, the auxiliary compensation circuit is implemented with a current source, which provides a high output impedance as seen by the other loop across the current transformer. As a result, when the auxiliary compensation circuit is providing a constant current output, interaction between the two compensation circuits is minimized.

By separating the compensation current into two subsystems, the design process can be divided into two problems which may be tailored to take advantage of the input signal characteristics. In this case, two compensation circuits add complexity to the system, but provide more flexible power and bandwidth trade-offs.

C. Feedback

Feedback is one of the key concepts that enables the proposed sensing system to work properly. This proposed system consists of two analog feedback loops and one digital feedback loop. The small compensation current uses analog feedback to keep the magnetic core in the zero-flux region. The second feedback loop ensures an accurate conversion between the command voltage and the compensation current. Both of these feedback loops act as minor loops within the digital feedback loop. The digital feedback enables flexible control of the entire process, and can be easily adapted for different input signal characteristics.

IV. Prototype Implementation

The prototype system was implemented according to the design introduced in §II. The system block diagram is shown in Fig. 6. The physical coupling of the subsystems occurs on a single toroidal core. The primary current to be measured passes through N_1 turns on the core. The cancellation current passes through N_2 turns, wound in the opposite direction. The residual current is measured by a closed-loop Hall sensor that utilizes N_3 additional turns. The N_2 and N_3 loops are co-wound to minimize leakage inductance. Typical values for our testing are $N_1 = 50$ and $N_2 = N_3 = 200$.

A. Residual Current Measurement

The residual current measurement is based on the closed-loop Hall-effect sensor shown in Fig. 4. The sensor drives an

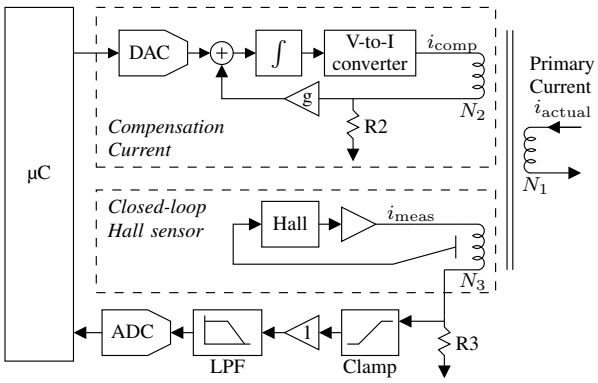

Fig. 6. Detailed block diagram of the prototype system.

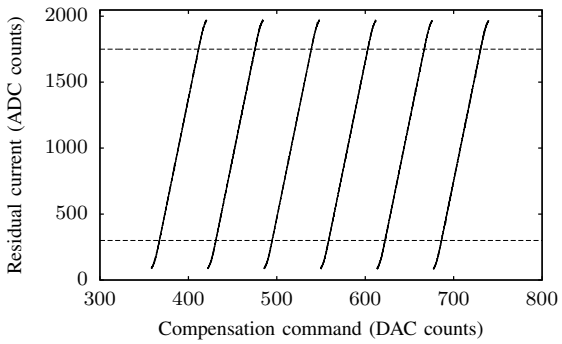

Fig. 7. Calibration curves showing 11-bit residual current measurement versus 10-bit compensation current command, at various fixed primary currents. The curves are generally linear with slope k_r and flatten out as the clamps begin to activate outside of the dashed lines.

output current such that the flux perceived by the Hall element is near zero. At this operating point, the temperature drift and offset of the Hall sensor are minimized. The output current is read by an 11-bit ADC to produce the residual measurement.

In our system, the Hall sensor is designed to measure over a small current range of approximately ± 2.5 A. If the input signal starts to exceed this range, the compensation current driver is separately commanded to cancel a portion of the flux in order to keep the residual sensor operating normally.

Fig. 7 shows measured calibration curves between the compensation current output and residual sensor input, for various operating points set by the primary current. The slope of each line corresponds to the constant k_r in (4). The dashed lines indicate the approximate measuring range of the ADC for the residual current. The digital controller attempts to maintain the window so that the residual current always falls within this range.

During a high current transient, the input current may temporarily exceed the ability of the system to compensate. To prevent the residual sensor from overloading in this condition, a clamp circuit is added at the output of the Hall sensor. This extra clamp current serves to cancel the primary current and limit maximum residual. The clamp current is not reflected in the ADC reading, causing the measured values to saturate, as shown shown in Fig. 7. After the overload condition, the clamp

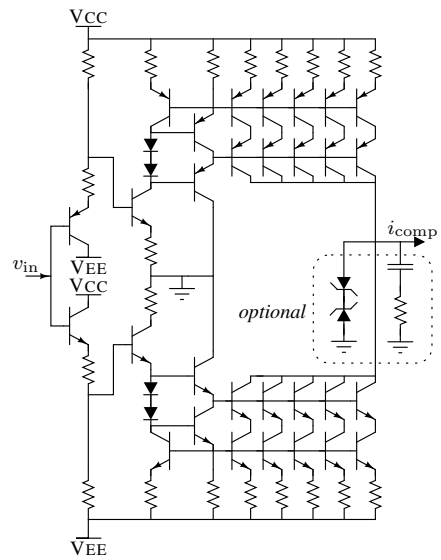

Fig. 8. Output stage of the compensation current subsystem, showing the OTA implementation.

deactivates and the Hall sensor returns to normal operation. The system utilizes a magnetic core with a low remnant flux to further minimize the offset error after experiencing such a transient.

B. Compensation Current

The compensation current driver uses a highly stable digital-to-analog converter to establish a voltage command reference. A closed-loop circuit, shown in Fig. 6, is designed to scale and convert the voltage command into the desired output current. This output current is co-wound on the core with the output from the closed-loop Hall sensor circuit. To minimize interaction between the two feedback loops, the output stage of the compensation circuit is high-impedance and appears as an open circuit to the residual sensor circuit.

The OTA design is shown in Fig. 8. In this implementation, the OTA includes a voltage buffer front-end to receive the voltage command from the compensation current feedback op-amp. The buffered command is used to establish a reference output current in the second stage. This reference current is replicated through a current mirror structure. The current mirror uses a cascode topology to improve the output impedance. The emitter degeneration resistors are added to scale the current and to prevent a thermal runaway condition. The OTA structure includes multiple output branches connected in parallel, in order to minimize the power dissipation per branch. Within each cascode branch, the transistor next to the rail sets up the mirrored current, and the cascode transistor acts as a current buffer. The power dissipation in each cascode branch will be concentrated at the cascode transistor. Therefore, the thermal effects on the mirrored current are reduced. Finally, the β-helper transistors are included to provide additional base current for the output stage.

The OTA output passes through N_2 turns on the core and is measured with a sense resistor. The analog feedback loop in

the compensation current subsystem serves to minimize error within the output stage. The output current measurement can optionally be provided back to the microcontroller through a low-bandwidth 24-bit ADC for calibration purposes.

C. Microcontroller

Control logic for the prototype is implemented using a Microchip dsPIC33FJ256GP710 microcontroller. It controls the sampling of the residual current measurement, implements the windowing algorithm used to set the compensation current, and communicates all data to a computer for analysis. The microcontroller also performs calibration at startup and on request.

1) Sampling: The ADC is sampled at 8 kHz, a rate chosen to match that used in existing non-intrusive load monitoring systems [13]. At each sample, the microcontroller calculates the total reconstructed current from the compensation command and the residual measurement, and transmits this data to the computer. If necessary, the compensation command is then changed to adjust measurement window.

The sampling interval has a direct influence on the slew rate capability of the system. If the residual current exceeds the window range, the measurement is clamped and the recombined output will be inaccurate. For a given operating point and windowing strategy, a maximum current excursion i_w can be observed within the current window before saturation. Given the sampling interval Δt and primary input slew rate $\frac{di}{dt}$, it is necessary that

$$\Delta t \cdot \frac{di}{dt} < i_w. \tag{8}$$

Thus, decreasing Δt, by increasing the sampling rate, has a corresponding linear effect on the maximum slew rate $\frac{di}{dt}$.

In practice, the limit on Δt is set by the response time of the hardware components and the processing speed of the microcontroller. Regardless of the sampling rate, the data reporting rate to the computer can be maintained at 8 kHz for compatibility.

2) Windowing Strategy: Using (4), the microcontroller can determine by how much a given change in DAC command will affect the sensor measurement at the ADC input. Assuming that the primary current i_{actual} remains constant, a pair of DAC and ADC values are related by

$$k_s(v_{\text{DAC},1} + k_r \cdot v_{\text{ADC},1}) = k_s(v_{\text{DAC},2} + k_r \cdot v_{\text{ADC},2}) \tag{9}$$

$$v_{\text{DAC},1} - v_{\text{DAC},2} = k_r(v_{\text{ADC},1} - v_{\text{ADC},2}) \tag{10}$$

Thus, to cause a change of ΔADC at the residual measurement, the DAC command should be changed by $k_r\Delta\text{ADC}$. The prototype implementation uses this approach to "recenter" the window whenever the ADC value begins to approach the clamp limits. This is depicted in Fig. 9. For example, when a sample x from the ADC exceeds a fixed upper limit of 1536, the compensation command is increased by $k_r(x - 768)$ so that the next sample is near 768.

The chosen target ADC values intentionally overshoot the center of the ADC range because it is expected that, in most cases, an increasing current will continue to increase. This provides some extra "headroom" for the common case, which in turn increases the maximum slew rate that the prototype can handle.

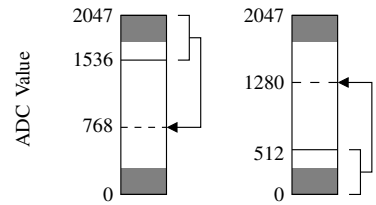

Fig. 9. Windowing approach in the prototype implementation. For input ADC values greater than 1536, the compensation current is changed such that the target ADC value is 768. For input ADC values less than 512, the target ADC value is 1280. The clamps are active in the shaded regions.

3) Communication: All data, including raw DAC and ADC values and calibration constants, are continuously sent to a computer via a full-speed USB link. In some configurations, the microcontroller may read the ADC more frequently than the samples are sent to the computer, and so status flags that indicate error states are also included independently. For example, one flag denotes whether the ADC value was ever observed in the clamped region, which indicates that the returned data for that sample may not be accurate to full resolution.

4) Calibration: In order to perform windowing accurately, the microcontroller needs to know the calibration constant k_r (§II-A) and the table LOOKUP (§II-B).

The value of k_r can be determined using the relationship in (10), if the primary current is constant. In the prototype implementation, the microcontroller assumes constant current and performs calibration at startup, or when triggered by the connected computer. Using an initial estimate $k_r = 1$, the calibration algorithm adaptively adjusts the estimate as it changes v_{DAC} to seek two specific v_{ADC} values corresponding to ADC inputs 512 and 1536. Once these DAC commands are found, each v_{ADC} is oversampled to reduce noise and a final accurate estimate of k_r is computed.

Table LOOKUP is used to map each low-resolution DAC command to its corresponding high-resolution stable output voltage. In the current prototype, this extended stability is simulated using an accurate DAC, and so the lookup is hard-coded to match the randomized low-order bits written to the DAC. However, the system supports an additional low-bandwidth 24-bit ADC for measuring the output compensation current. This calibration ADC could be used to measure and fill the LOOKUP entries for each possible DAC output, in the absence of a hard-coded table.

Finally, to convert the final output of the physically-windowed current sensor to amperes, the scaling factor k_s is used. It is not directly needed by the microcontroller logic, and is currently calibrated by the computer in post-processing using known test values from a Keithley 2400 Sourcemeter.

V. Prototype Results

Various aspects of the prototype physically-windowed current sensor system have been tested.

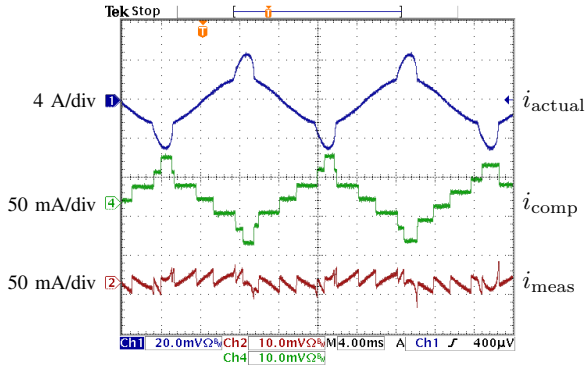

Fig. 10. Oscilloscope traces showing the measured primary, compensation, and residual measurement currents while the prototype physically-windowed current sensor is in normal operation.

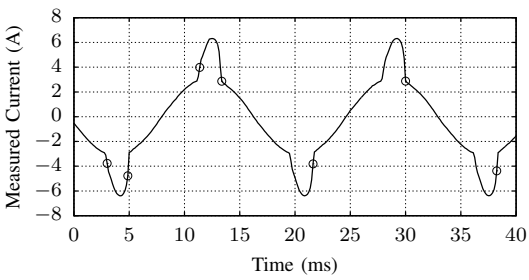

Fig. 11. Reconstructed current from the sensor. Circled points indicate individual samples that are known to be potentially inaccurate because the residual current was in the clamped region of the sensor window.

A. Full system functionality

Basic functionality was tested by constructing a test load consisting of an incandescent light bulb and a personal computer, which together draw power at both the fundamental and third harmonics of the line frequency. Fig. 10 shows the waveforms as measured by external test equipment. The input current is i_{actual}, the generated compensation current is i_{comp}, and the residual current is i_{meas}.

The reconstructed output of the sensor system for the same test load, based on data reported by the microcontroller, is shown in Fig. 11. In some cases, the high slew rate associated with the third harmonic content in the load caused the residual current measurement to exceed its window and enter the region where the clamps are active. The recombined data at these samples is known to be potentially inaccurate because of this. In the figure, these specific samples are circled. Note that they do not occur uniformly on every line cycle, because such excursions from the window depend on the varying relationship between sample time, slew rate, and the current window position.

B. Static resolution tests

The maximum resolution of the sensor system was characterized by analyzing the static performance. For this test, a Keithley 2400 Sourcemeter was used to supply various dc currents. These currents were passed through the sensor $N_1 = 50$ times to create the primary current i_{actual}. Each effective

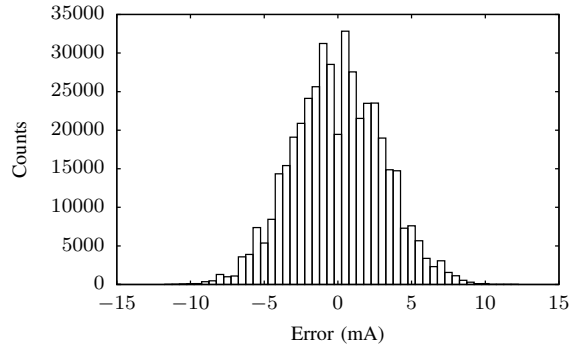

Fig. 12. Histogram of the measured errors during a test of dc performance. 91% of the samples fall within ±5 mA, which gives an accuracy over the full ±80 A range of approximately one part in 2^{14}.

current level was chosen at random from a ±25 A range. Once the test current stabilized, the reconstructed output from the prototype system was sampled at 8 kHz for approximately 110 ms. Approximately 500 unique test current levels were applied in total. A histogram of the resulting error between the Keithley reported output and the reconstructed sensor output is shown in Fig. 12. Typical errors for each sample are less than ±5 mA. Over the full 160 A range of the compensation current driver, this 10 mA range translates into an effective resolution of

$$\log_2(160/0.01) = 13.996 \text{ bits} \tag{11}$$

In the prototype system, the DAC command for the current compensation is 10 bits, while the ADC input from the residual measurement is 11 bits. This result of nearly 14 bits demonstrates the concept of using physical windowing to extend the sensor resolution over a larger range.

C. Dynamic resolution tests

The ability to resolve small signals while tracking a large signal was evaluated by creating a test load consisting of an incandescent lamp bulb in parallel with the Keithley 2400 Sourcemeter. For this test, the change in the envelope of the measured lamp ac waveform was examined as various small test currents were injected through the sensor using the Keithley source. The injected current was cycled between 0 mA, 20 mA, and 10 mA. The resulting reconstructed waveform is shown in Fig. 13. The small change in dc level can be seen in the detail shown in part (c). Like the static resolution test, this shows a resolution of approximately 10 mA.

D. Residual sensor transient response

In order to prevent drift in the output, the residual sensor employs a current clamp that prevents the toroidal core from saturating. The transient response of the residual sensor was tested by applying a large instantaneous current of 20 A through $N_1 = 5$ turns. This results in an effective primary current of 100 A, significantly greater than the typical operating window for the residual. This test simulates the case where a large input transient is seen before the compensation current is

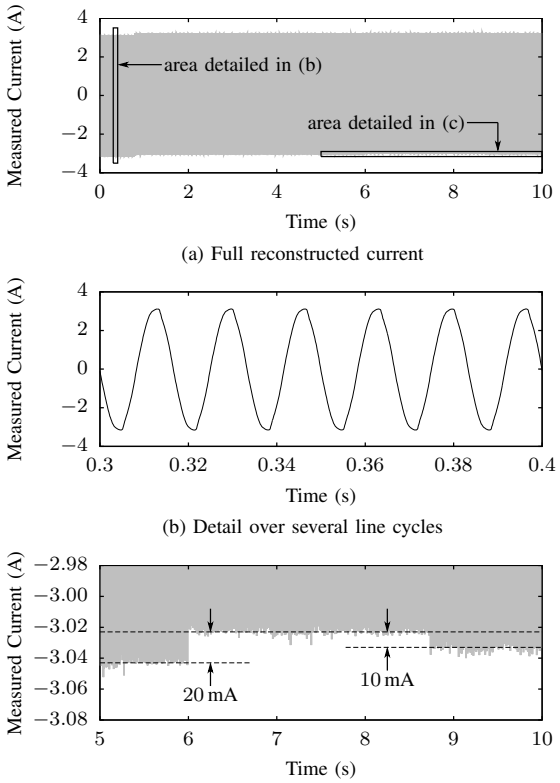

(a) Full reconstructed current

(b) Detail over several line cycles

(c) Detail of a small dc change

Fig. 13. Example of measuring a small dc current on top of a large ac current. The ac current is from a light bulb and the dc offset is added by a Keithley 2400 Sourcemeter, measured in parallel. Steps of 10 mA are resolvable in the reconstructed sensor output.

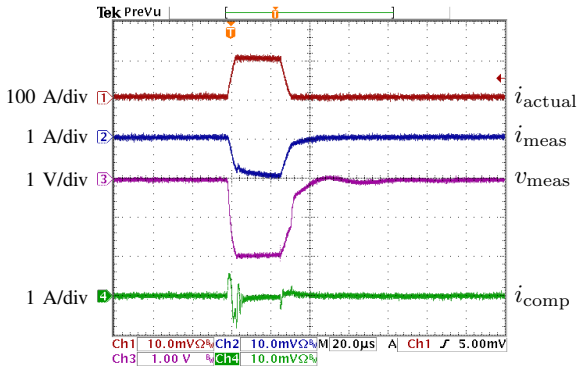

Fig. 14. System response during a high current transient. A pulse of primary current i_{actual} =100 A is applied for 25 µs. The clamp activates, limiting the residual current in the core. After deactivating, the offset measured at the core is less than 5 mV. The compensation current is also shown, demonstrating that it quickly stabilizes back to the commanded value after an induced change.

applied. The results are shown in Fig. 14. During the transient, the clamp activates, providing necessary current to keep the core near the zero-flux operating point. When the transient disappears, due to either a change in input or a change of the compensation current, the clamp deactivates and the residual current measurement resumes normal behavior. The offset drift in the residual sensor output V_{meas} is less than 5 mV after the transient, demonstrating that hysteresis loss in the core was minimized.

VI. Conclusions and Further Work

The prototype sensor has demonstrated that the physical windowing approach is able to extend the range of an 11-bit current sensor with a 10-bit compensation command to provide approximately 14-bit resolution in the reconstructed output.

This windowing technique has many uses in smart grid and other applications where there is a need to measure fast, small signals on top of slow, large signals. The non-intrusive load monitor suggests many example uses, such as finding the high-frequency principal slot harmonics for motor diagnostics, or examining very small loads in aggregate power metering. The same technique is expected to be applicable to other physical systems, such as pressure monitors and strain gauges, with example uses including water system monitoring and wing flutter measurement.

Acknowledgements

This research was funded by The Grainger Foundation, the BP-MIT Research Alliance, the US Department of Energy ARPA-E, the MIT Sea Grant College Program, and by Dr. Manny Landsman.

References

[1] S. B. Leeb, S. R. Shaw, and J. L. Kirtley, "Transient event detection in spectral envelope estimates for nonintrusive load monitoring," *IEEE Trans. Power Del.*, vol. 10, no. 3, pp. 1200–1210, Jul 1995.

[2] J. S. Ramsey, S. B. Leeb, T. DeNucci, J. Paris, M. Obar, R. Cox, C. Laughman, and T. J. McCoy, "Shipboard applications of non-intrusive load monitoring," in *American Society of Naval Engineers Reconfigurability and Survivability Symposium*, Atlantic Beach, Florida, February 2005.

[3] T. DeNucci, R. Cox, S. B. Leeb, J. Paris, T. J. McCoy, C. Laughman, and W. Greene, "Diagnostic indicators for shipboard systems using non-intrusive load monitoring," in *IEEE Electric Ship Technologies Symposium*, Philadelphia, Pennsylvania, July 2005.

[4] C. R. Laughman, S. R. Shaw, S. B. Leeb, L. K. Norford, R. W. Cox, K. D. Lee, and P. Armstrong, "Power signature analysis," *IEEE Power and Energy Magazine*, pp. 56–63, March 2003.

[5] R. W. Cox, P. Bennett, D. McKay, J. Paris, and S. B. Leeb, "Using the non-intrusive load monitor for shipboard supervisory control," in *IEEE Electric Ship Technologies Symposium*, Arlington, VA, May 2007.

[6] D. Son and J. D. Seivert, "A new current sensor based on the measurement of the apparent coercive field strength," *IEEE Trans. Instrum. Meas.*, vol. 38, no. 6, pp. 1080–1082, Dec 1989.

[7] S. Ogasawara, K. Murata, and H. Akagi, "A digital current sensor for pwm inverters," in *Industry Applications Society Annual Meeting, 1992., Conference Record of the 1992 IEEE*, vol. 1, Oct 1992, pp. 949–955.

[8] T. Sonoda, R. Ueda, and K. Koga, "An ac and dc current sensor of high accuracy," *IEEE Trans. Ind. Appl.*, vol. 28, no. 5, pp. 1087–1094, Sept/Oct 1992.

[9] J. Pankau, D. Leggate, D. Schlegel, R. Kerkman, and G. Shibiniski, "High frequency modeling of current sensors," *IEEE Trans. Ind. Appl.*, vol. 35, no. 6, pp. 1374–1382, Nov/Dec 1999.

[10] D. Li and G. Chen, "A wide bandwidth current probe based on rogowski coil and hall sensor," in *Power Electronics and Motion Control Conference, 2006. IPEMC 2006. CES/IEEE 5th International*, vol. 2, Aug 2006, pp. 1–5.

[11] J. Lenz and A. S. Edelstein, "Magnetic sensors and their applications," *IEEE Sensors J.*, vol. 6, no. 3, pp. 631–649, Jun 2006.

[12] M. M. Ponjavić and R. Durić, "Nonlinear modeling of the self-oscillating fluxgate current sensor," *IEEE Sensors J.*, vol. 7, no. 11, pp. 1546–1553, Nov 2007.

[13] J. Paris, Z. Remscrim, K. Douglas, S. B. Leeb, R. W. Cox, S. T. Gavin, S. G. Coe, J. R. Haag, and A. Goshorn, "Scalability of non-intrusive load monitoring for shipboard applications," in *American Society of Naval Engineers Day 2009*, National Harbor, Maryland, April 2009.

[14] C. Moreland, F. Murden, M. Elliott, J. Young, M. Hensley, and R. Stop, "A 14-bit 100-msample/s subranging adc," *IEEE J. Solid-State Circuits*, vol. 35, no. 12, pp. 1791–1798, Dec 2000.

[15] K. D. Hurst and T. G. Habetler, "Sensorless speed measurement using current harmonic spectral estimation in induction machine drives," *IEEE Trans. Power Electron.*, vol. 11, no. 1, pp. 66–73, 1996.